Journal of Power Sources 608 (2024) 234689

Contents lists available at ScienceDirect

Journal of Power Sources

journal homepage: www.elsevier.com/locate/jpowsour

Multifaceted effects of ring fusion on the stability of charged dialkoxyarene redoxmers

Zhiguang Li [a,b,c,e], Heonjae Jeong [d,e,1], Xiaoting Fang [a,b,c], Yuyue Zhao [a,c,e], Lily A. Robertson [c,e], Jingjing Zhang [c,e], Ilya A. Shkrob [c,e,**], Lei Cheng [d,e], Xiaoliang Wei [a,*], Lu Zhang [c,e,***]

[a] Department of Mechanical and Energy Engineering, Indiana University-Purdue University Indianapolis, 723 West Michigan Street, Indianapolis, IN, 46202, USA
[b] School of Mechanical Engineering, Purdue University, 585 Purdue Mall, West Lafayette, IN, 47907, USA
[c] Chemical Sciences and Engineering Division, Argonne National Laboratory, 9700 South Cass Avenue, Lemont, IL 60439, USA
[d] Materials Science Division, Argonne National Laboratory, 9700 South Cass Avenue, Lemont, IL, 60439, USA
[e] Joint Center for Energy Storage Research, Argonne National Laboratory, Lemont, IL, 60439, USA

HIGHLIGHTS

- Ring fusion has competing effects on the stability of dimethoxyarene radical cations.
- Steric stress can modulate molecular conformation and compromise stability.
- Second-order neutralization of radical cations can occur for planar molecules.
- Electrochemical titration can decouple charge and discharge capacities.

GRAPHICAL ABSTRACT

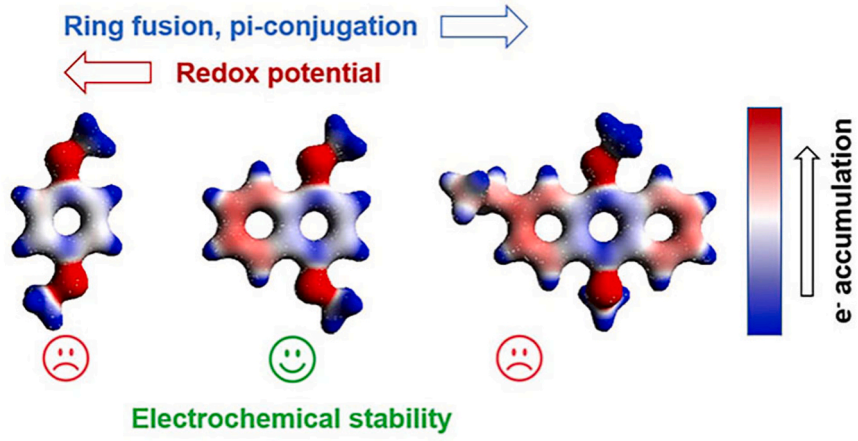

ARTICLE INFO

Keywords:
Nonaqueous redox flow battery
organic redox molecules
Ring fusion

ABSTRACT

Due to their almost unlimited scalability, redox flow batteries can make versatile and affordable energy storage systems. Redox active materials (redoxmers) in these batteries largely define their electrochemical performance, including the life span of the battery that depends on the stability of charged redoxmers. In this study, we examine the effects of expanding the π-system in the arene rings on the chemical stability of dialkoxyarene redoxmers that are used to store positive charge in RFBs. When 1,4-dimethoxybenzene is π-extended to 1,4-

* Corresponding author.
** Corresponding author.
*** Corresponding author.
E-mail addresses: Shkrob@anl.gov (I.A. Shkrob), xwei18@iupui.edu (X. Wei), zhanglu77@gmail.com (L. Zhang).
[1] Present Address: Dr. Heonjae Jeong: Department of Electronic Engineering, Gachon University, 1342 Seongnam-daero, Sujeong-gu, Seongnam-si, Gyeonggi-do 13120, South Korea.

https://doi.org/10.1016/j.jpowsour.2024.234689
Received 17 November 2023; Received in revised form 9 April 2024; Accepted 6 May 2024
Available online 9 May 2024

Stability
Steric strain

dimethoxynaphthalene, a lower redox potential, improved kinetic stability, and longer cycling life are observed. However, when an additional ring is fused to make 9,10-dimethoxyanthracene, the radical cation undergoes rapid *O*-dealkylation possibly due to increased steric strain that drives methoxy out of the arene plane thus breaking the π-conjugation with O 2p orbitals. On the other hand, the planar structure of 1,4-dimethoxynaphthalene may facilitate second-order reactions of radical cations leading to their neutralization in the bulk. Our study suggests that extending the π-system changes reactivity in multiple (sometimes, opposite) ways, so lowering the oxidation potential through π-conjugation to improve redoxmer stability should be pursued with caution.

1. Introduction

Energy storage systems play a crucial role in the growing integration of intermittent renewable energies, reliable enhancement of grid efficiency, and steady transformation of the global energy landscape. Among the variety of storage approaches, redox flow batteries (RFBs) hold particular promise [1,2]. In an RFB, the redox-active materials, denoted as redoxmers, are dissolved in liquid electrolytes that are circulated through porous electrodes to enable electrochemical reactions. Such a cell architecture spatially decouples energy storage from charge generation, offering ready scalability and system flexibility that make RFBs attractive for stationary storage applications. Organic redoxmers are widely used in RFBs as the energy-bearing materials, primarily because their structural diversity and tunability can offer an opportunity for facile property enhancement [3–5]. Although aqueous electrolytes have advantages of high conductivity, non-flammability, and cost-effectiveness, nonaqueous RFBs have been pursued as their wider electrochemically stable window (up to 5 V) can enable more redoxmer candidates, higher operation voltage, and greater energy density [6,7]. However, pushing the redox potentials to the extreme carries a risk of reduced stability of charged molecules, while RFBs are expected to have long storage times of 4–20 h and be used over thousands of cycles, which requires exceptional stability of the redoxmers in all states of charge (SOCs). Designing organic molecules that remain sufficiently stable in such operating regimes has proven to be a major challenge [8].

A nonaqueous electrolyte includes an organic solvent and a supporting salt, both of which can potentially react with the charged organic redoxmer [9]. Ring fusion onto the redox core of organic structures has been demonstrated as an effective strategy to improve the stability of organic redoxmers. The working mechanism lies in the two effects of such π-extension: (i) it hinders the chemical attack by incoming agents and provides steric protection; and (ii) it induces conjugative charge delocalization to protect the vulnerable moieties in the redoxmer core. For example, azobenzene-based organic redoxmers achieved long cycle life in nonaqueous RFBs, because the two end benzene rings stabilize the reversible redox chemistry of the azo core (-N═N-) [10]. In a separate study, a ketone anolyte core and a phenothiazine catholyte core were incorporated into a single conjugated molecule, creating an organic bipolar redoxmer with mutual stabilization of both redox activities [11]. The benzene ring substitute on the PTIO core improves the stability of a charged nitronyl nitroxide radical [12]. The π-extension strategy has also been explored in aqueous RFBs to stabilize organic redoxmers such as viologen, phenazine, quinone, etc. [13–15], demonstrating its versatile power in improving structural stability.

In this study, we examine the competing effects of ring fusion for dialkoxyarene-based organic catholyte redoxmers. 1,4-Dimethoxybenzene (DMB) is a popular catholyte scaffold due to molecular simplicity, high redox potential, and ease of structural engineering to tailor solubility and stability [16,17]. Progressive introduction of fused benzene rings to yield 1,4-dimethoxynaphthalene (DMN) and then 9, 10-dimethoxyanthracene (DMA) results in increased stability for the former but poor stability for the latter molecule after it becomes charged. To understand this trend, a combination of electrochemical analysis, post-mortem chemical characterization, and computational modeling were carried out. A novel "electrochemical titration" method was demonstrated to separate different mechanisms for degradation of cell performance. The results indicate that steric strain induced by full ring fusion accelerates the *O*-demethylation side reaction, which outweighs the stabilizing effects of π-system extension; however, when this strain is eliminated in DMN, a second-order neutralization reaction becomes prevalent, so some steric protection is desired to prevent such reactions. Our finding suggests that ring fusion can have opposite effects on different reaction channels for radical cation decay, highlighting a critical need for more cautious factor balancing to achieve durable organic redoxmers.

2. Results and discussion

Structurally homologous redoxmers are required to study the ring fusion effects on stability, as their radical cations share similar degradation pathways. 1,4-Dimethoxybenzene (DMB) and 1,4-dimethoxynaphthalene (DMN) are commercially available. 9,10-dimethoxyanthracene has a near-zero solubility in the solvent used in this study, so 2-ethyl-9,10-dimethoxyanthracene (EDMA) with an improved solubility was used instead.

When charged in electrolyte, these dimethoxyarenes yield radical cations by losing an electron. Cyclic voltammetry (CV) was used to determine the reversibility of this redox reaction. Fig. 1 shows iR-compensated CV curves obtained with a glassy carbon electrode at a concentration of 5 mM redoxmer in 0.5 M tetraethylammonium bis (trifluoromethanesulfonyl)imide (TEATFSI) in dry acetonitrile. Table S1summarizes the major electrochemical parameters obtained from these CV scans: the half-wave potential (E), peak separation (ΔE), peak current ratio (i_a/i_c), and diffusion coefficient (D) (see Fig. S1).

All three redoxmers exhibit $1e^-$ redox activity as seen from the ~70 mV peak separations at the slowest scan rate of 10 mV s^{-1} (ideally, it is 59 mV separation for a reversible $1e^-$ reaction). DMB has the highest redox potential of 0.96 V vs. Ag/Ag^+. When the π-system is expanded, the redox potential decreases by 0.24 V for DMN (to 0.72 V vs. Ag/Ag^+) and by 0.34 V for EDMA (reaching 0.62 V vs. Ag/Ag^+). These observed changes in the redox potential correspond well with the estimates obtained using density functional theory (DFT) calculations. As shown in Table S2, the average partial atomic charge and spin densities for radical cations decrease as the size of the π-system increases from DMB to EDMA. The excess charge and spin are shared between more atoms, which explains the trend in the redox potential. Finally, the ratio of the anodic and cathodic peak currents (i_a/i_c) is used to estimate electrochemical reversibility. Among the three redoxmers, DMB has a peak current ratio of 1.46 and thus is not considered electrochemically reversible. Fusion of an additional ring to DMN decreases the i_a/i_c ratio to 1.03, which suggests electrochemical reversibility. However, further ring fusion to EDMA yields the i_a/i_c ratio of 1.22 suggesting compromised reversibility despite a greater extent of conjugation. The cyclic voltammograms of these redoxmers obtained using other supporting salts show the same trend in electrochemical reversibility (Fig. S2), so the inferior electrochemical stability of EDMA cannot be due to a reaction with electrolyte ions. An implication from these experiments is that the charged EDMA may have lower chemical stability compared to the charged DMN under the CV condition, which is opposite to the expected trend.

To further characterize the electrochemical stability for the three

redoxmers, electrochemical cycling was conducted in symmetric H cells under the same conditions. In the H-cell setup, two identical solutions containing 5 mM redoxmer with a 0.5 M TEATFSI supporting electrolyte were used in the two cell compartments; after the first half cycle, the counter compartment was replaced with a fresh solution to remove reduction products. Then, the charging and discharging were conducted at a 3C charge rate and were terminated when the working electrode potential met the preset voltage limits, or when the capacity reached half of the theoretical value, i.e., at 50 % state of charge (SOC), whichever came first. With this cycling protocol, the capacity can decrease only when >50 % of the redoxmer is decomposed, facilitating direct comparison between the redoxmers.

The cycling capacity and coulombic efficiency (CE) for DMB, DMN and EMDA are plotted in Fig. 2a–c, and the voltage profile data are available in Fig. S3. DMB shows rapid capacity fading after only 3 cycles and negligible discharge capacity. This cycling behavior suggests poor stability of the radical cation, which agrees with a previous report for DMB-based redoxmers [18]. Considering the more stable derivatives that have additional substituents at the 2- and 5-positions in the benzene ring, the lack of steric protection in this ring is the major reason for the rapid degradation of charged DMB (see below). In contrast, DMN displays a significantly improved cycling performance with near-100 % CEs and stable capacity for 147 cycles that corresponds to 48 h, followed by gradual capacity fading. This improvement reflects the greater stability of the DMN radical cation. However, for EDMA, rapid capacity fading was observed after only 3 cycles with low discharge capacity and CE, indicating rapid decay of the EDMA radical cation albeit with additional ring fusion. Fig. 2d–e shows the post-cycling CVs for redoxmer solutions in the working electrode chamber. For DMB and EDMA, there is major loss of the redoxmers after only a few cycles. In contrast, there is still intact DMN present after 156 cycles. It is noted that these redoxmers display similar cycling behaviors when LiTFSI was used as the supporting salt (Fig. S4). Thus, the H-cell cycling accords well with CV measurements to demonstrate short lifetimes for the radical cations of DMB and EDMA and a longer lifetime for the radical cation of DMN.

The radical cation of DMB, i.e., $DMB^{+\bullet}$, can be decomposed via *O*-demethylation to form quinone (route I in Fig. S5), disproportionation (route ii), C–C ring addition (route iii), and reactions with organic solvent and/or salt (route iv). Prior studies indicate that C–C ring addition coupled with deprotonation is the dominant reaction pathway for DMB; it is this reaction that is impeded using steric protection groups in the benzene ring [19–23]. For DMN and EDMA, fusion of the benzene ring (s) largely precludes this ring addition and they are expected to have increasing stability. DMN follows this trend well, but EDMA does not despite its more extensive ring fusion. Thus, competing effects must exist from ring fusion. To obtain more insight on the underlying mechanism, a post-mortem chemical analysis of the cycled DMN and EDMA was conducted using gas chromatography - mass spectroscopy (GC-MS) to identify reaction products. The cycled electrolytes underwent a workout procedure consisting of solvent removal under reduced pressure, washing with water to remove LiTFSI salt, and extraction of organic molecules using dichloromethane. The collected organic layer was dried and concentrated before the chromatographic analysis. Fig. 3 shows the chromatographic peaks and mass spectra of the pristine and cycled solutions of DMN and EDMA. No dimer or oligomer C–C ring addition products were observed in the extracted material, showing the effectiveness of blocking this pathway by ring fusion. A concern may be whether dichloromethane can extract the ring addition products. In fact, the scenario that acetonitrile soluble ring addition products are not soluble in dichloromethane is quite unlikely. These side products are C–C bound ring dimers or oligomers, formed by the radical cation attacking the ring of the parent molecule with the loss of a proton [21, 24], and they should be extractable by dichloromethane. The same analytical protocol was used in our previous study and was proven quite effective [18]. A chromatographic peak from the parent DMN is obvious, and 1,4-naphthoquinone (NQ) is a major volatile product whose identity is validated by the GC-MS of commercial NQ in Fig. 3a. The NQ peak is rather weak and corresponds to a reaction yield of ca. 3 %. Conversely, for EDMA, a substantial yield (38 %) of 2-ethylanthracene-9,10-dione was observed (Fig. 3c). The dramatically different yields of the quinones suggest the *O*-demethylation as the main decomposition mechanism for EDMA, but not for DMN. Another pronounced result from the GC-MS is the presence of intense neutral redoxmer (DMN and EDMA) peaks. These peaks may come partially from the unreacted redoxmers in H-cell cycling, but we also observed a significant amount of neutralization of the radical cations in the aged samples.

To elucidate the different decomposition behaviors, DFT analyses were performed to calculate the gas-phase Gibbs free energies (ΔG) for the parasitic reactions (Table S2). While DMN exhibits somewhat higher ΔG for the *O*-demethylation reaction than EDMA, what matters for kinetics most are the activation energies for the reaction that reflect an important structural difference between the two molecules. Fig. 4 presents the optimized gas phase molecular geometries for the neutral state and radical cation of DMN and EDMA. For DMN, the O–C bonds in the methoxy groups lie in the same plane as the arene ring, as indicated by the 0°/180° of the dihedral angle (φC-C-*O*-C). This planar conformation leads to good conjugation of the arene π-system and O 2p orbitals. In contrast, EDMA exhibits φC-C-*O*-C dihedral angles of 90.7°/89.3° in the neutral state and of 31.5°/148.5° at carbon-9 and 77.6°/102.4° at carbon-10 in the radical cation. The reason for this out-of-plane rotation of the methoxy group in EDMA is that the C–H bonds in the *ortho* positions introduce spatial strain forcing this group out and breaking π-conjugation with the O 2p orbital. Similar dihedral angles are observed in the computed optimized geometries and crystal structures for analogous 9,10-dialkoxyanthracene derivatives (Figs. S6 and S7). The structural strain in EDMA eases the *O*-dealkylation reaction as this strain is removed from the resulting aroxyl radical. In contrast, in DMN, the two methoxy groups can rotate away from the *ortho* C–H bonds and remain in the arene plane, which explains their greater stability of the radical cation. Such stress-induced destabilization has also been

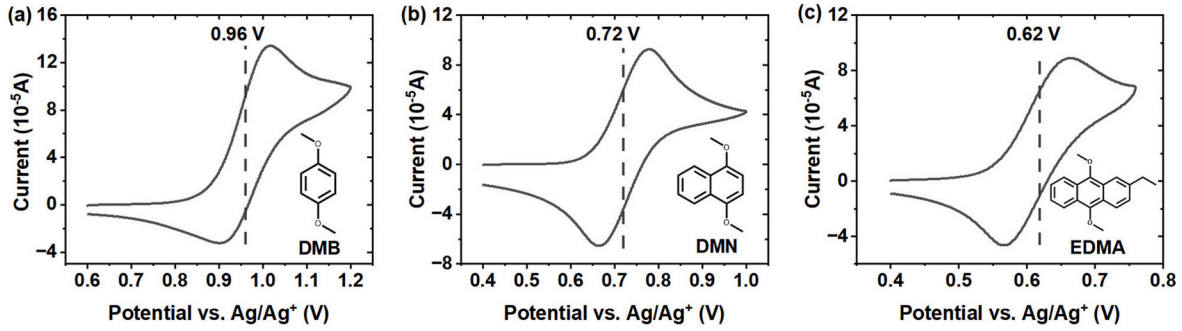

Fig. 1. Cyclic voltammograms obtained for 5 mM (a) DMB, (b) DMN, and (c) EDMA in 0.5 M TEATFSI in acetonitrile at a scan rate of 100 mV s^{-1}. The molecular structures are given in the insets.

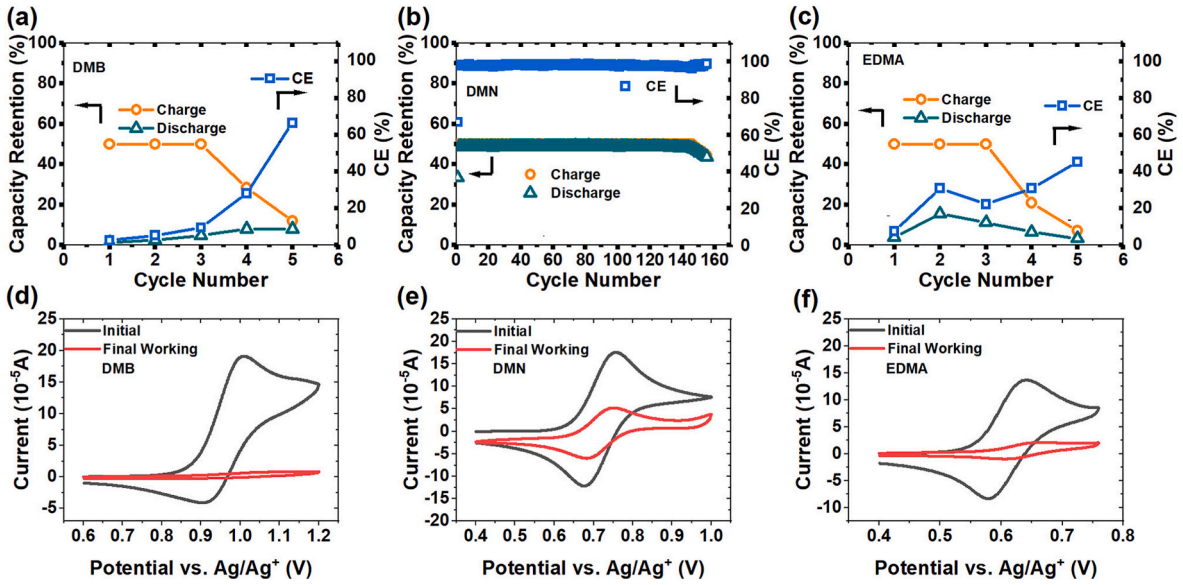

Fig. 2. Normalized capacity and CE profiles for H-cells containing 5 mM (a) DMB, (b) DMN, and (c) EDMA with 0.5 M TEATFSI in acetonitrile. Capacity is normalized by the theoretical capacity for $1e^-$ reaction. CV spectra of (d) DMB, (e) DMN, and (f) EDMA were measured before and after cycling in the working electrode chamber.

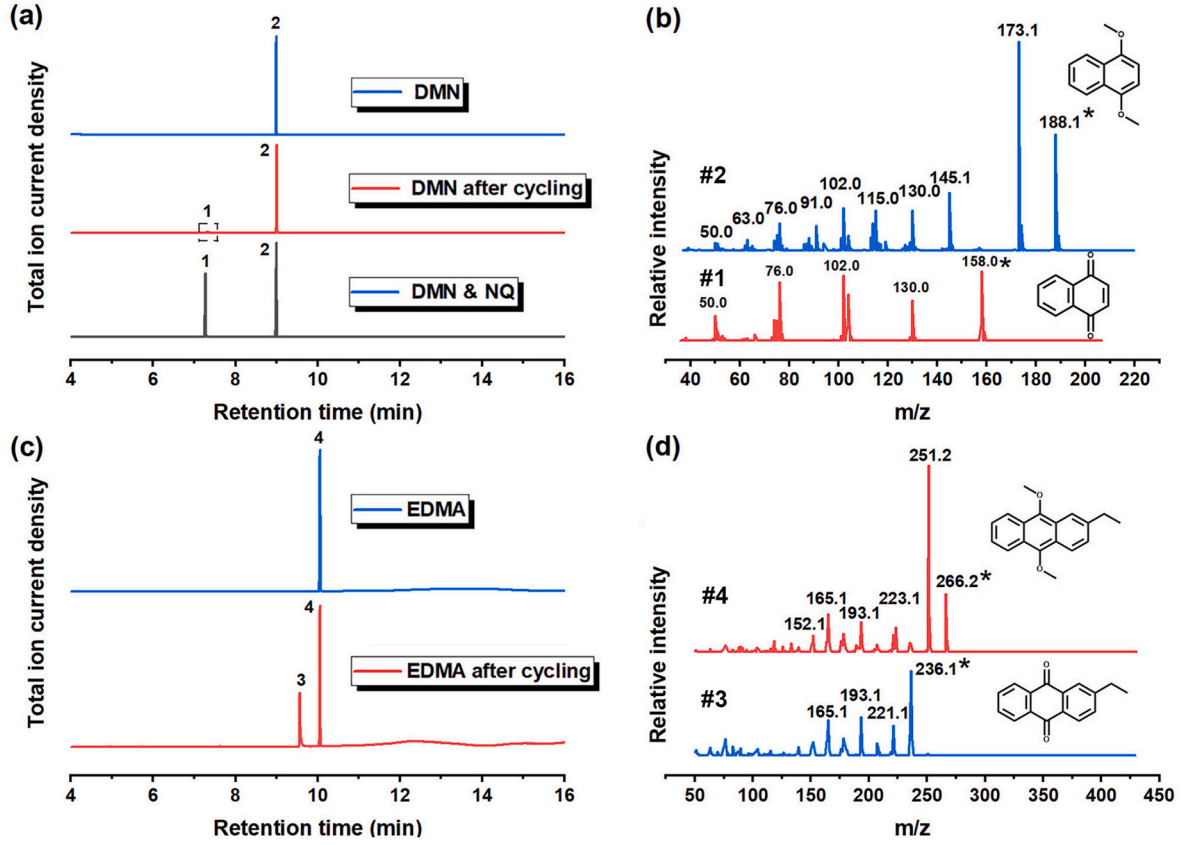

Fig. 3. Post-cycling GC-MS analyses of DMN and EDMA. (a) The total ion current chromatograms and (b) mass spectra of the pristine DMN solutions (peak 2), cycled DMN solutions, and 1:1 M ratio of the pristine DMN and NQ solutions (peak 1). (c,d) The same for EDMA (peak 4) and 2-ethylanthracene-9,10-dione (peak 3). The asterisk labels the characteristic mass-to-charge (m/z) peaks for each compound.

observed in 2,6-dialkylated and annulated DMBs, which supports our argument [17,18,23]. By our DFT calculation, the structural strain in EDMA lowers the reaction barrier for *O*-demethylation by 0.24 eV.

While these structural considerations offer valuable insights in the difference between DMN and EDMA, the *O*-demethylation is just one of the several parasitic reactions. To probe other reaction channels, electron paramagnetic resonance (EPR) spectroscopy was performed to obtain the decay kinetics of $DMN^{+\bullet}$. The results are plotted in Fig. 5a

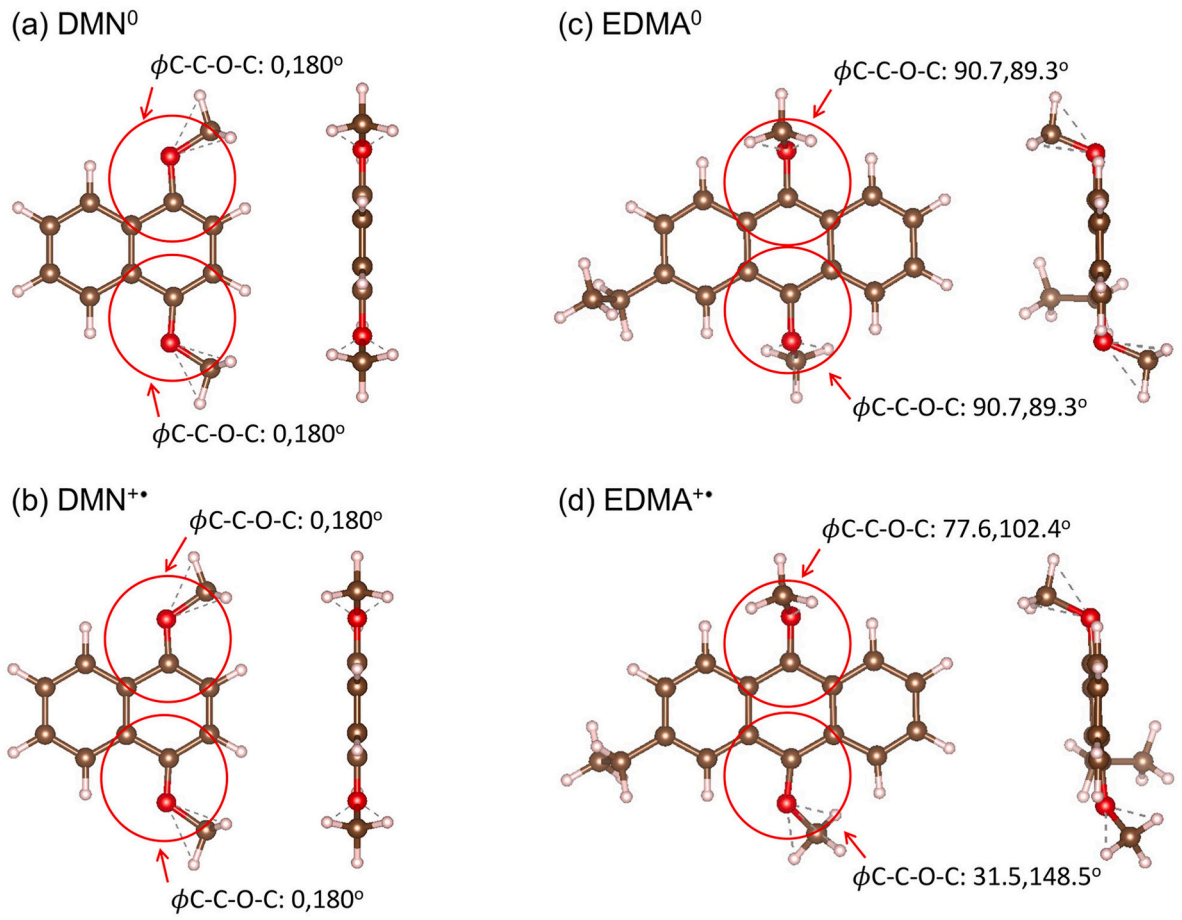

Fig. 4. Computed optimized geometries in gas phase: (a) DMN, (b) $DMN^{+\bullet}$, (c) EDMA, and (d) $EDMA^{+\bullet}$. Each panel contains top and side views. Red circles label φC-C-*O*-C dihedral angles. (For interpretation of the references to colour in this figure legend, the reader is referred to the Web version of this article.)

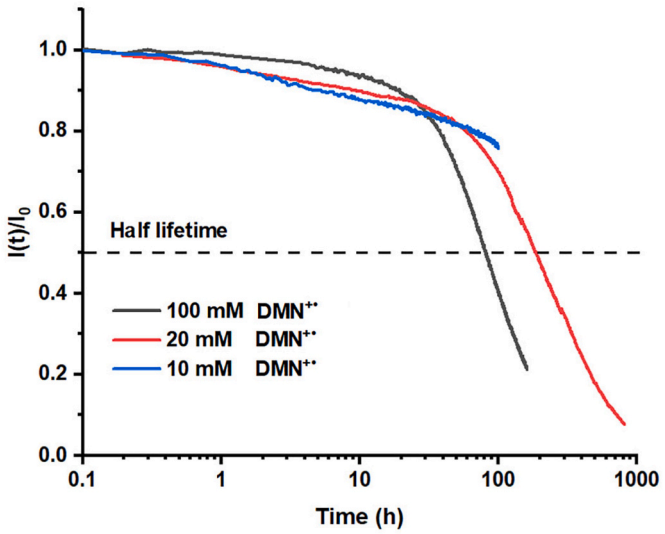

Fig. 5. EPR measurement of decay kinetics for the electrochemically prepared $DMN^{+\bullet}$ at different concentrations. The $t_{1/2}$ of 10 mM $DMN^{+\bullet}$ is obtained by fitting (Fig. S8). Note the logarithmic time scale.

and S8. (The decay of $EDMA^{+\bullet}$ was too fast to allow such time-resolved EPR measurements). Due to fast spin exchange at concentrations ≥10 mM, the first-derivative EPR spectra of $DMN^{+\bullet}$ are unresolved singlet lines. These EPR spectra were doubly integrated and normalized to estimate the relative loss of paramagnetic species. As the initial concentration of $DMN^{+\bullet}$ increases from 10 mM to 20 mM and on to 100 mM, the half-life time $t_{1/2}$ for the decay of the EPR signal decreases from 480 h to 187 h and then to 63 h, respectively. This concentration dependence suggests that the decay of $DMN^{+\bullet}$ is of mixed first and second orders with respect to it, and the second-order reaction is apparently the more dominant one. This kinetic behavior contrasts with our observations for sterically protected dialkoxybenzenes (shown in Fig. S9), for which the lifetime of radical cation did not change significantly with the concentration of the radical cation, conforming to a (pseudo) first order reaction [23]. The first-order reaction would correspond to the *O*-demethylation that yields the NQ and the parent DMN through disproportionation of the secondary aroxyl radicals derived from DMN (route i in Fig. S5). However, according to GC-MS, this reaction is nearly negligible as the yield of NQ is low. The origins of the second-order reaction are not well understood. One possibility is the disproportionation of $DMN^{+\bullet}$ yielding the parent DMN and unstable dication DMN^{2+} (route ii in Fig. S5). However, the expected low molecular weight products of dication decomposition were not observed by NMR and GC-MS. Other possibilities may include reactions of $DMN^{+\bullet}$ with secondary products of $DMN^{+\bullet}$ decomposition. We leave the mechanism an open problem, but note that this second order reaction, which is a variety of disproportionation, can potentially recover DMN as a neutral molecule.

If neutralization occurs, the regenerated DMN molecule can be charged again, so the discharge capacity (carried by the radical cations) and charge capacity (carried by the parent molecules) could significantly differ [25,26]. With that in mind, an electrochemical "titration" test was designed to demonstrate this difference. A 100 mM DMN

electrolyte was fully charged electrochemically in an H-cell using a constant-current, constant voltage protocol (Fig. 6a) and the resulting $DMN^{+\bullet}$ solution was removed from the cell and stored separately. At set delay times of 0, 72, 120 and 214 h, aliquots of the charged solution were collected, diluted with 0.5 M LiTFSI electrolyte and paired with fresh DMN solutions of the same molarity in symmetric H-cells. An electrochemical discharge-charge cycle was performed to each of these H-cells to extract the respective discharge and charge capacities (Fig. 6b–e), which were normalized to the theoretical capacity stored in this solution and plotted against the delay time (Fig. 6f). We stress that the redox material crossover was negligible over the duration of this test (Section S3). It is seen that, during storage, the discharge capacity decays in the same way as the EPR signal, as both of these quantities are proportional to the residual concentration of $DMN^{+\bullet}$. In contrast, the charge capacity (proportional to the concentration of the parent molecules after full discharge) decays much slower, suggesting the presence of extra DMN that was not recovered by electrochemically discharging of $DMN^{+\bullet}$. The decoupling of charge and discharge capacities provides direct evidence for regeneration of the parent DMN from the decayed $DMN^{+\bullet}$. Comparing these time profiles, we inferred that ~80 % of radical cations were converted back to DMN during 200 h of charge storage. This result suggests that the calendar life decay also contributes to the cycle life decay and that a larger reversible capacity as compared to the apparent capacities from cycling can be expected. If this regeneration also occurs for DMB and EDMA, it would account for the ability to recharge after near-zero discharge observed in the first few cycles for DMB and EDMA in Fig. 2a and c. As their radical cations decayed too fast for the "titration" method, we could not verify this conjecture, but it is likely that the reaction is not specific to DMN.

The results of these combined analyses demonstrate that ring fusion has multifaceted effects on the chemical properties of charged dialkoxyarene redoxmers. The π-extension can decrease the redox potential and improve the stability via spin and charge delocalization, but excessive ring fusion may cause spatial over-crowding and induce unwanted steric strain to the alkoxy substituents, which accelerates *O*-dealkylation. With the terminal DMB ring, $DMN^{+\bullet}$ has the planar structure, so this *O*-dealkylation is slow; however, the radical cation reacts with itself (or a product of decomposition) to yield a neutral molecule, so the chemical stability is still compromised. A flow cell test using DMN and 2,1,3-benzothiadiazole [27] as the catholyte and anolyte redoxmers, respectively, reflects this point. A capacity fading was observed over 50 cycles even with 0.1 M redoxmers (Section S4 and Fig. S10), suggesting a limited cycle life when high SOC was reached. Nevertheless, despite the insufficient stability, our study reveals an under-addressed but critical design pitfall in the development of organic redoxmers with improved stability. Caution should be used when implementing ring fusion.

3. Conclusion

In this study, we inquire how the expansion of the rings in dialkoxyarenes affects their performance as the catholyte redoxmers in nonaqueous RFBs. Simplemindedly, one can expect that lowering of the redox potential and spreading of the excess charge and spin over the π-system would make the extended radical cation more stable by leaving less energy needed for breaking a particular chemical bond. Our study suggests that this way of thinking can be useful but ultimately deficient, as multiple competing reaction pathways exist for a radical cation: The structural modifications can have different effects on the different pathways.

For dialkoxyarenes, one of these reaction pathways is the ring addition by which the unprotected radical cation of DMB rapidly decays. Ring extension provides robust protection against this reaction pathway, but for a price. We found that the radical cation of EDMA (and, by extension, other derivatives of 9,10-dialkoxyanthracene) becomes unstable to C–O bond scission. The structural straining incurred by the fully extended ring forces the methoxy groups to adopt an out-of-plane orientation resulting in reduced π-conjugation with the O 2p orbitals and facilitating the *O*-dealkylation. In DMN and other arene molecules with the terminal DMN rings, this straining does not occur; however, while the ring addition and *O*-dealkylation are both inhibited, that still does not make the radical cation stable in the long run. Specifically, our kinetic experiments suggest that the electrochemically generated radical cations of DMN decay by neutralization, albeit with unclear reaction pathways. This slow neutralization reaction was not observed for EDMA and other dialkoxyarenes that rapidly decay via *O*-dealkylation well before this reaction becomes significant. This structural insight into the multifaceted role of ring extension and substitution is the main conclusion of our study. The competing effects of ring fusion must be considered when rationalizing structural design to achieve stable redoxmers.

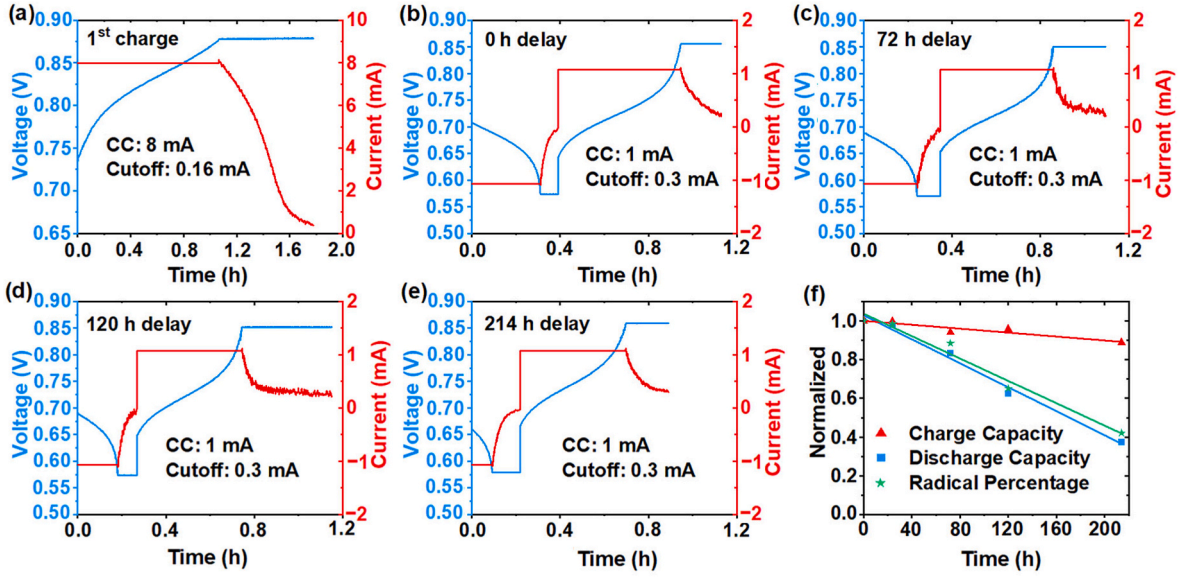

Fig. 6. Electrochemical "titration" of aged $DMN^{+\bullet}$: (a) Voltage (left) and current (right) profiles for charging up 100 mM DMN in 0.5 M LiTFSI in acetonitrile; (b–e) Voltage and current profiles of titration cells at 0, 72, 120, and 214 h after the initial charging; (f) The relative loss of charge and discharge capacities vs. storage time, compared with the EPR decay kinetics.

4. Experimental

4.1. Materials and methods

1,4-Dimethoxybenzene (DMB, 99 %), 1,4-dimethoxynaphthalene (DMN, 97 %), 2-ethyl-9,10-dimethoxyanthracene (EDMA, 97 %), lithium bis(trifluoromethane)sulfonimide (LiTFSI, 99.95 %), tetraethyl ammonium bis(trifluoromethane)sulfonimidate (TEATFSI, 99 %), and acetonitrile (electronic grade, 99.999 %) were purchased from Sigma-Aldrich. LiTFSI and TEATFSI were dried at 120 °C in vacuo for 8 h before use. DMB, DMN and EDMA were dried under vacuum at room temperature before use. Acetonitrile was dried over 3 Å molecular sieves for two days before use. All chemicals were stored in an argon-filled glovebox ($O_2 < 5$ ppm, $H_2O < 0.5$ ppm) where electrochemical measurements were conducted.

^1H and ^{13}C NMR spectra were obtained using 300 MHz Avance III Bruker spectrometer. For GC-MS analyses, 1 μL liquid sample was loaded on an HP-5MS (bore 0.25 μm, length 30 m) column using an Agilent Technologies Model 7890B chromatograph equipped with a Model 5977 mass detector. The typical program included a 20 min holdup at 50 °C, followed by 20 °C/min ramp to 250 °C followed by another 20 min holdup. UV–vis spectra of the radical cations were collected using an Olis 14c Carry spectrometer. The freshly prepared samples were sealed in a quartz cuvette with 1 mm optical path.

4.2. Electrochemical characterizations

*i*R-compensated cyclic voltammograms was obtained in a three-electrode cell using the potential scanning rates between 10 and 500 mV s^{-1} (CHI760D workstation, CH Instruments, TX). A glassy carbon disk (CHI 104) and Pt wire (CHI 115) were used as working and counter electrodes, respectively. $Ag/AgNO_3$ (10 mM in acetonitrile) was used as a pseudo-reference electrode.

Electrochemical cycling was performed in symmetric H-cells using the approach described in Ref. [28] Each cell chamber contained a magnetically stirred 4 mL electrolyte and a reticulated vitreous carbon electrode (45 PPI, ERG Aerospace Corporation). A porous ceramic disk served as a separator (P5 frit, Adams and Chittenden). An $Ag/AgNO_3$ electrode was placed near the working electrode to control the potential. The solution in the counter chamber was replaced with a fresh solution after the first charge. The H-cells were cycled at a constant rate of 3C until the set capacity or potential limit was reached, whichever came first.

4.3. DFT calculations

DFT calculations were performed using the Gaussian 16 and the 3-parameter hybrid Becke 88 exchange functional with Lee-Yang-Parr correlation functional (B3LYP) and 6–311++G(d,p) basis set [29–32]. The acetonitrile solvent (dielectric permittivity $\epsilon = 35.7$) was simulated using the polarizable continuum model [33]. Geometry optimization and vibration frequency calculations were performed to compute the Gibbs free energies at 298 K. The oxidation potential (E_{ox}) in V vs. Ag/Ag^+ were calculated using Eq. (1) below:

$$E_{ox} = const + \frac{\Delta G^{ox}}{F} \quad (1)$$

where F is the Faraday constant; *const* is the potential difference between the standard hydrogen electrode and the Ag/Ag^+ reference electrode, which is *ca.* −4.78 V; ΔG^{ox} is the difference between the Gibbs free energies of the oxidized and neutral solvated molecules, respectively.

4.4. EPR measurements

The $DMN^{+\bullet}$ samples were freshly prepared by charging DMN solutions in H-cells at 3C to the full nominal capacity. The charged solution was placed in a glass capillary and contained in a glass tube with a piston seal (Wilmad-Lab Glass model 734-LPV-7). Continuous wave EPR measurements were performed using a Bruker ESP300E X-band spectrometer operating at ~9.4347 GHz with 2 mW microwave power and 0.2 G modulation at 100 kHz. The EPR spectra were recorded at the constant time intervals, centered, background corrected, and doubly integrated.

4.5. Electrochemical titration

For stability measurements, the H-cell was filled with 4 mL of an acetonitrile solution containing 100 mM DMN and 0.5 M LiTFSI in each compartment. This cell was charged at 3C until it reached the potential limit of 0.88 V vs. Ag/Ag^+, followed by a potential hold until the current decreased below C/50. The fully charged solution was then removed and stored in a sealed vial. At set time intervals, a 200 μL aliquot was diluted by 1:20 v/v with 0.5 M LiTFSI/acetonitrile and placed into the working chamber, while the counter chamber was filled with a fresh DMN solution of the same molarity. The two chambers were magnetically stirred for 30 min before cycling. The cell was discharged at ~2C until the potential of 0.56 V vs. Ag/Ag^+ was reached and then held at this potential until the current rate decreased below C/50. The discharge was followed by a galvanostatic charge and potentiostatic hold at 0.87 V vs. Ag/Ag^+.

CRediT authorship contribution statement

Zhiguang Li: Writing – original draft, Visualization, Methodology, Investigation, Data curation. **Heonjae Jeong:** Writing – review & editing, Investigation. **Xiaoting Fang:** Writing – review & editing, Investigation. **Yuyue Zhao:** Writing – review & editing, Investigation. **Lily A. Robertson:** Writing – review & editing, Investigation. **Jingjing Zhang:** Writing – review & editing, Investigation. **Ilya A. Shkrob:** Writing – review & editing, Methodology, Investigation, Formal analysis. **Lei Cheng:** Writing – review & editing, Investigation. **Xiaoliang Wei:** Writing – review & editing, Supervision, Funding acquisition, Formal analysis, Conceptualization. **Lu Zhang:** Writing – review & editing, Supervision, Funding acquisition, Formal analysis, Conceptualization.

Declaration of competing interest

The authors declare that they have no known competing financial interests or personal relationships that could have appeared to influence the work reported in this paper.

Data availability

Data will be made available on request.

Acknowledgments

This work was partially supported by the Joint Center for Energy Storage Research (JCESR), an Energy Innovation Hub funded by the U.S. Department of Energy, Office of Science, Basic Energy Sciences. The authors also thank financial support from the U.S. National Science Foundation (Award No. CHE-2055222) and from the U.S. Department of Energy, Office of Science, Small Business Innovation Research (Award No. 077040-00002B). The submitted manuscript has been created by UChicago Argonne, LLC, Operator of Argonne National Laboratory ("Argonne"). Argonne, a U.S. Department of Energy Office of Science laboratory, is operated under Contract No. DE-AC02-06CH11357. The U.S. Government retains for itself, and others acting on its behalf, a paid-up nonexclusive, irrevocable worldwide license in said article to reproduce, prepare derivative works, distribute copies to the public, and perform publicly and display publicly, by or on behalf of the

Government.

Appendix A. Supplementary data

Supplementary data to this article can be found online at https://doi.org/10.1016/j.jpowsour.2024.234689.

References

[1] B. Dunn, H. Kamath, J.M. Tarascon, Science 334 (2011) 928–935.
[2] Z.G. Yang, J.L. Zhang, M.C.W. Kintner-Meyer, X.C. Lu, D.W. Choi, J.P. Lemmon, J. Liu, Chem Rev 111 (2011) 3577–3613.
[3] X.L. Wei, W.X. Pan, W.T. Duan, A. Hollas, Z. Yang, B. Li, Z.M. Nie, J. Liu, D. Reed, W. Wang, V. Sprenkle, ACS Energy Lett. 2 (2017) 2187–2204.
[4] J. Winsberg, T. Hagemann, T. Janoschka, M.D. Hager, U.S. Schubert, Angew Chem Int Edit 56 (2017) 686–711.
[5] J.A. Luo, B. Hu, M.W. Hu, Y. Zhao, T.L. Liu, ACS Energy Lett. 4 (2019) 2220–2240.
[6] G.L. Soloveichik, Chem Rev 115 (2015) 11533–11558.
[7] K. Gong, Q.R. Fang, S. Gu, S.F.Y. Li, Y.S. Yan, Energ Environ Sci 8 (2015) 3515–3530.
[8] M. Li, Z. Rhodes, J.R. Cabrera-Pardo, S.D. Minteer, Sustain Energ Fuels 4 (2020) 4370–4389.
[9] X.L. Wei, W. Xu, J.H. Huang, L. Zhang, E. Walter, C. Lawrence, M. Vijayakumar, W. A. Henderson, T.B. Liu, L. Cosimbescu, B. Li, V. Sprenkle, W. Wang, Angew Chem Int Edit 54 (2015) 8684–8687.
[10] L.Y. Zhang, Y.M. Qian, R.Z. Feng, Y. Ding, X.H. Zu, C.K. Zhang, X.L. Guo, W. Wang, G.H. Yu, Nat. Commun. 11 (2020). ARTN 3843.
[11] Y. Liu, G.L. Dai, Y.Y. Chen, R. Wang, H.M. Li, X.L. Shi, X.H. Zhang, Y. Xu, Y. Zhao, ACS Energy Lett. 7 (2022) 1274–1283.
[12] W.T. Duan, R.S. Vemuri, J.D. Milshtein, S. Laramie, R.D. Dmello, J.H. Huang, L. Zhang, D.H. Hu, M. Vijayakumar, W. Wang, J. Liu, R.M. Darling, L. Thompson, K. Smith, J.S. Moore, F.R. Brushett, X.L. Wei, J. Mater. Chem. A 4 (2016) 5448–5456.
[13] J. Luo, B. Hu, C. Debruler, T.L. Liu, Angew. Chem. 57 (2017) 231–235.
[14] C. Wang, X. Li, B. Yu, Y. Wang, Z. Yang, H. Wang, H. Lin, J. Ma, G. Li, Z. Jin, ACS Energy Lett. 5 (2020) 411–417.
[15] B. Huskinson, M.P. Marshak, C. Suh, S. Er, M.R. Gerhardt, C.J. Galvin, X.D. Chen, A. Aspuru-Guzik, R.G. Gordon, M.J. Aziz, Nature 505 (2014) 195–198.
[16] J.H. Huang, L. Cheng, R.S. Assary, P.Q. Wang, Z. Xue, A.K. Burrell, L.A. Curtiss, L. Zhang, Adv. Energy Mater. 5 (2015) 1401782.
[17] J. Zhang, Z. Yang, I.A. Shkrob, R.S. Assary, S.o. Tung, B. Silcox, W. Duan, J. Zhang, C.C. Su, B. Hu, B. Pan, C. Liao, Z. Zhang, W. Wang, L.A. Curtiss, L.T. Thompson, X. Wei, L. Zhang, Adv. Energy Mater. 7 (2017) 1701272.
[18] J.H. Huang, B.F. Pan, W.T. Duan, X.L. Wei, R.S. Assary, L. Su, F.R. Brushett, L. Cheng, C. Liao, M.S. Ferrandon, W. Wang, Z.C. Zhang, A.K. Burrell, L.A. Curtiss, I.A. Shkrob, J.S. Moore, L. Zhang, Sci Rep-Uk 6 (2016). ARTN 32102.
[19] J.S. Foos, S.M. Erker, L.M. Rembetsy, J. Electrochem. Soc. 133 (1986) 836–841.
[20] V. Leberre, L. Angely, J. Simonet, G. Mousset, M. Bellec, J. Electroanal. Chem. 218 (1987) 173–185.
[21] Z.H. Chen, Q.Z. Wang, K. Amine, J. Electrochem. Soc. 153 (2006) A2215–A2219.
[22] R.S. Assary, L. Zhang, J. Huang, L.A. Curtiss, J. Phys. Chem. C 120 (2016) 14531–14538.
[23] J. Zhang, I.A. Shkrob, R.S. Assary, S.o. Tung, B. Silcox, L.A. Curtiss, L.T. Thompson, L. Zhang, J. Phys. Chem. C 121 (2017) 23347–23358.
[24] J. Simonet, Pure Appl. Chem. 70 (1998) 1253–1257.
[25] N.H. Attanayake, T.M. Suduwella, Y. Yan, A.P. Kaur, Z. Liang, M.S. Sanford, S. A. Odom, J. Phys. Chem. C 125 (2021) 14170–14179.
[26] B. Silcox, J. Zhang, I.A. Shkrob, L. Thompson, L. Zhang, J. Phys. Chem. C 123 (2019) 16516–16524.
[27] W.T. Duan, J.H. Huang, J.A. Kowalski, I.A. Shkrob, M. Vijayakumar, E. Walter, B. F. Pan, Z. Yang, J.D. Milshtein, B. Li, C. Liao, Z.C. Zhang, W. Wang, J. Liu, J. S. Moore, F.R. Brushett, L. Zhang, X.L. Wei, ACS Energy Lett. 2 (2017) 1156–1161.
[28] J. Zhang, J. Huang, L.A. Robertson, I.A. Shkrob, L. Zhang, J. Power Sources 397 (2018) 214–222.
[29] M.J. Frisch, G.W. Trucks, H.B. Schlegel, G.E. Scuseria, M.A. Robb, J.R. Cheeseman, G. Scalmani, V. Barone, G.A. Petersson, H. Nakatsuji, X.C. Li, M. Marenich, J.A V, B.G. Bloino, R. Janesko, B. Gomperts, H.P. Mennucci, J.V. Hratchian, A.F. Ortiz, J. L. Izmaylov, D. Sonnenberg, F.L. Williams-Young, F.F. Ding, J.P. Egidi, B. Goings, A. Petrone, T. Henderson, D. Ranasinghe, V.G Zakrzewski, J. Gao, N. Rega, G. Zheng, W. Liang, M. Hada, M. Ehara, K. Toyota, R. Fukuda, J. Hasegawa, M. Ishida, T. Nakajima, Y. Honda, O. Kitao, H. Nakai, T. Vreven, K. Throssell, J. A Montgomery Jr., J.E. Peralta, F. Ogliaro, M.J. Bearpark, J.J. Heyd, E.N. Brothers, K.N. Kudin, V.N. Staroverov, T.A. Keith, R. Kobayashi, J. Normand, K. Raghavachari, A.P. Rendell, J.C. Burant, S.S. Iyengar, J. Tomasi, M. Cossi, J. M. Millam, M. Klene, C. Adamo, R. Cammi, J.W. Ochterski, R.L. Martin, K. Morokuma, O. Farkas, J.B. Foresman, D.J. Fox, Gaussian 16, revision C.01, 2016. Wallingford CT.
[30] A.D. Becke, J. Chem. Phys. 98 (1993) 5648–5652.
[31] A.D. Becke, Phys. Rev. A 38 (1988) 3098–3100.
[32] C. Lee, W. Yang, R.G. Parr, Phys. Rev. B 37 (1988) 785–789.
[33] V. Barone, M. Cossi, J. Phys. Chem. A 102 (1998) 1995–2001.